Environmental Science & Technology

pubs.acs.org/est

Article

Acid–Base Properties of Cis-Vacant Montmorillonite Edge Surfaces: A Combined First-Principles Molecular Dynamics and Surface Complexation Modeling Approach

Pengyuan Gao, Xiandong Liu,* Zhijun Guo, and Christophe Tournassat*

Cite This: *Environ. Sci. Technol.* 2023, 57, 1342–1352

Read Online

ACCESS | Metrics & More | Article Recommendations | Supporting Information

ABSTRACT: Montmorillonite layer edge surfaces have pH-dependent properties, which arises from the acid–base reactivity of their surface functional groups. Edge surface acidity (with intrinsic reaction equilibrium constant, pK_a) is a chemical property that is affected by crystal structure. While a cis-vacant structure predominates in natural montmorillonites, prior molecular-level studies assume a centrosymmetric trans-vacant configuration, which potentially leads to an incorrect prediction of montmorillonite acid–base surface properties. We computed intrinsic acidity constants of the surface sites of a montmorillonite layer with a cis-vacant structure using the first-principles molecular dynamics-based vertical energy gap method. We evaluated pK_a values for both non-substituted and Mg-substituted layers on common edge surfaces (i.e., surfaces perpendicular to [010], [0$\bar{1}$0], [110], and [$\bar{1}$10] crystallographic directions). The functional groups ≡Si(OH), ≡Al(OH$_2$)$_2$/≡Al(OH)(OH$_2$), and ≡SiO(OH)Al sites on surfaces perpendicular to [010] and [0$\bar{1}$0] and ≡Si(OH)^U, ≡Si(OH)^L, ≡Al(OH$_2$), and ≡Al(OH$_2$)$_2$ on surfaces perpendicular to [110] and [$\bar{1}$10] determine the proton reactivity of non-substituted cis-vacant edge surfaces. Moreover, the structural OH sites on edge surfaces had extremely high pK_a values, which do not show reactivity at a common pH. Meanwhile, Mg^{2+} substitution results in an increase in pK_a values at local or adjacent sites, in which the effect is limited by the distance between the sites. A surface complexation model was built with predicted pK_a values, which enabled us to predict surface properties as a function of pH and ionic strength. Edge surface charge of both trans- and cis-vacant models has little dependence on Mg^{2+} substitutions, but the dependence on the crystal plane orientation is strong. In particular, at pH below 7, edge surfaces are positively or negatively charged depending on their orientation. Implications of these findings on contaminant adsorption by smectites are discussed.

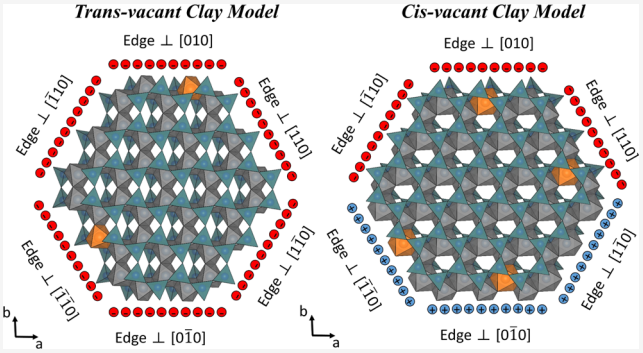

KEYWORDS: *first-principles molecular dynamics, clay, montmorillonite, cis-vacant, trans-vacant, pK_a, surface complexation modeling*

1. INTRODUCTION

High adsorption capacity of clay minerals plays a key role in nutrient cycling in soils[1] and in the retardation of heavy metals, oxyanions, and organic pollutants' migration in natural and engineered environments.[2,3] In particular, clay materials are an essential part of most multi-barrier systems envisioned for nuclear waste storage under consideration worldwide.[4] An accurate prediction of metal ion mobility in clay-rich environments is dependent on the development of adsorption models. Surface complexation model (SCM) links surface speciation to adsorption process and has been applied to describe the adsorption behaviors of a wide range of metal ions.[5]

The representative structure of clay minerals consists of an edge-sharing octahedral sheet connected to two corner-sharing tetrahedral sheets to form the 2:1 (i.e., TOT, tetrahedron–octahedral–tetrahedral) layer type.[4] Because of their layered structure, clay minerals exhibit two kinds of surfaces, basal and edge surfaces (Figure 1), with much contrasted adsorption properties: while basal surfaces interact with adsorbates mostly through electrostatic interaction, edge surfaces have amphoteric properties and can bind adsorbates through surface complexation.[4,6] Ideally, the reactivity description of SCM adsorption sites should be rooted in the actual structural properties of surface sites.

A key for understanding interfacial properties of clay minerals' edge surfaces is their acid–base reactivity.[7−9] The acid–base chemistry of edge surfaces is complicated because of

Received: September 30, 2022
Revised: December 16, 2022
Accepted: December 16, 2022
Published: January 10, 2023

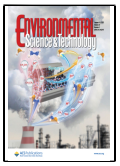

https://doi.org/10.1021/acs.est.2c07171
Environ. Sci. Technol. 2023, 57, 1342–1352

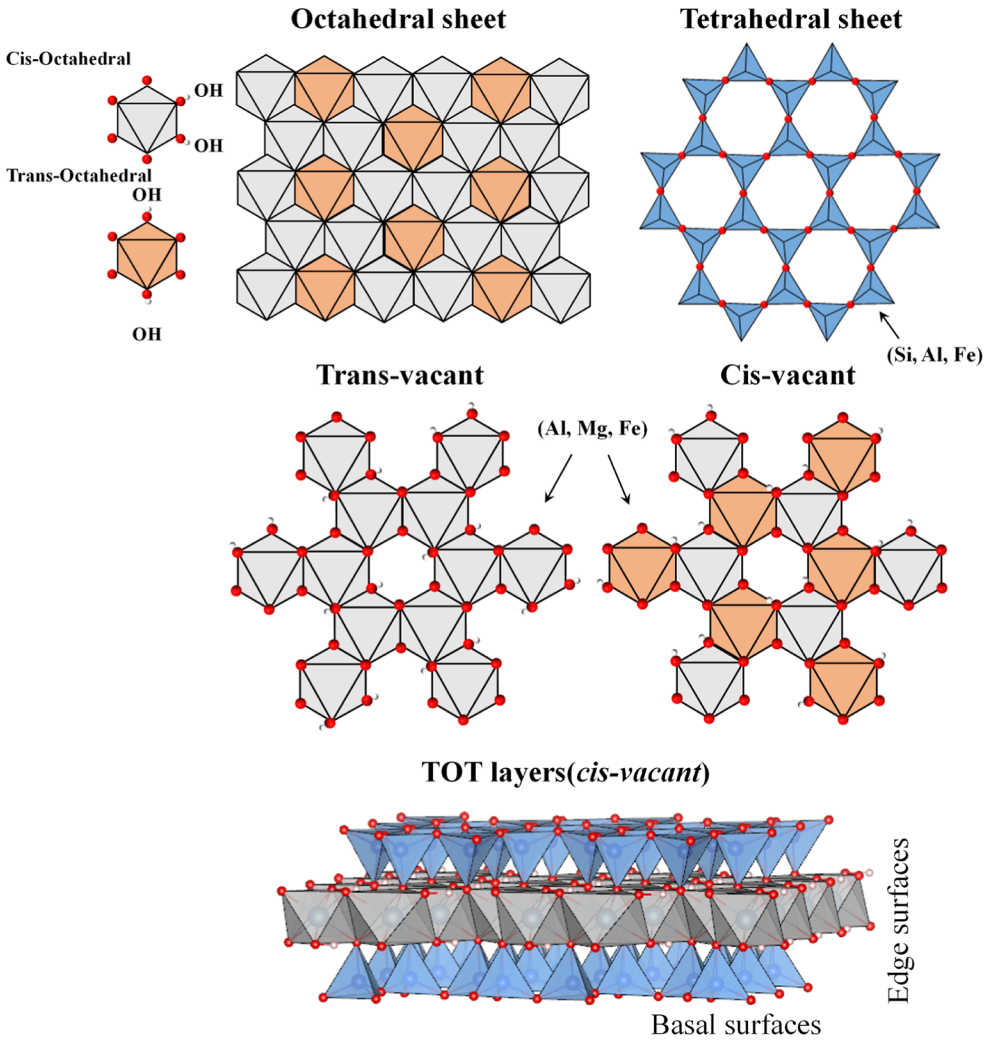

Figure 1. From top to bottom: octahedral and tetrahedral sheets, octahedral sheet with trans-vacant and cis-vacant configurations, TOT layers.

the very heterogeneous nature of surface sites in terms of chemistry and structural position.[10] Potentiometric titration has been extensively carried out to study the acid−base reactivity of clay mineral.[11−20] Among others, Baeyens and Bradbury[11] and Duc et al.[15] established acid−base titration data sets of montmorillonite, and SCMs based on thermodynamic equilibrium equations were developed to simulate titration data,[12,21] using fitted pK_a for protons on edge surfaces. More recently, pK_a values derived from ab initio calculations have been made available,[22−30] and Tournassat et al.[21] pooled these newly available pK_a values in an SCM to yield reasonable prediction of the titration data of montmorillonite edge surfaces. The representativeness of these pK_a values is, however, questionable because of an additional structural peculiarity of clay mineral layers.[21]

In a TOT layer, each octahedral site is surrounded by two OH groups and four O atoms, but not all octahedral sites have the same geometry regarding the positions of OH groups. Trans-octahedra have OH groups on opposite corners, while *cis*-octahedra have OH groups on adjacent corners.[31,32] Consequently, a TOT layers may be either trans-vacant with pure *trans*-octahedra in the octahedral sheet or cis-vacant with half *cis*-octahedra and half *trans*-octahedra (Figure 1). Montmorillonite is a typical dioctahedral smectite that exhibits either cis- or trans-vacant structures, but cis-vacant structures are the most common in natural samples widely used in research studies, such as Wyoming montmorillonites available at the Source Clays Repository or Kunipia montmorillonite.[33,34] The cis-vacant structure of crystallographic planes was observed for Kunipia montmorillonite by using scanning transmission electron microscopy.[34] Tournassat et al.[21] pointed out that the theoretical estimates of intrinsic pK_a values were carried out on the basis of a trans-vacant model, whereas experimental titration and adsorption data were obtained on montmorillonite samples with a cis-vacant structure. Because the structure of a clay mineral determines its intrinsic physical and chemical properties, the differences between cis- and trans-vacant configurations inevitably lead to different surface properties. Cis-vacant structures are not centrosymmetric (Figure 1),[31] which indicates that the edges perpendicular to [010], [0$\bar{1}$0], [110], and [$\bar{1}$10] crystallographic directions are different. In addition, different positions of structural OH groups and isomorphic substitutions lead to more complex edge surface groups.[35,36] Whether these differences in structure cause different surface charging behaviors of montmorillonite had not been determined yet.

Theoretical estimates of the intrinsic pK_a values of edge surface sites have been based on bond-valence theories.[37] However, the obtained pK_a values were sensitive to model assumptions and did not reproduce the experimental titration

https://doi.org/10.1021/acs.est.2c07171
Environ. Sci. Technol. 2023, 57, 1342−1352

data.[36,38] First principles calculation provides a new research method for pK_a estimation.[39,40] In recent years, the first-principles molecular dynamics (FPMD) based vertical energy gap method has been proved a powerful tool to accurately calculate the intrinsic pK_a values of mineral surfaces.[22−27,30] Liu et al. have published a series of works about intrinsic pK_a values of surfaces perpendicular to [010] and [110] for a trans-vacant TOT layer.[22−25] The method has also been successfully applied to mineral surface OH groups including rutile, quartz, gibbsite, and kaolinite.[25−29] However, to the best of our knowledge, the cis-vacant clay edge surface properties of montmorillonite have not been reported.

In this work, we calculated the pK_a values of 2:1-type cis-vacant clay edge surfaces perpendicular to [010], [0$\bar{1}$0], [110], and [$\bar{1}\bar{1}$0] directions. The influence of Mg^{2+} substitution on acid−base properties was also investigated. The atomic-level acidity constants were then applied to construct an SCM for edge surfaces of a cis-vacant layer. By comparing our results with the previous pK_a values and SCM models of trans-vacant layer edge surfaces, we elucidated the difference between cis- and trans-vacant clay edge surfaces' acid−base properties. This study provides fundamental information for further multi-scale study of the interfacial processes of 2:1-type clay minerals, for example, the adsorption of contaminants on clay minerals.

2. METHODOLOGY

2.1. Models. The optimized primitive unit cell parameters of cis-vacant 2:1 dioctahedral phyllosilicates are a = 5.22 Å, b = 9.04 Å, c = 10.09 Å, and α = 89.82°, β = 99.55°, γ = 90.02°.[31] The hydrated edge surface models including two unit cells were placed in 3D periodically repeated orthorhombic boxes (12.45 Å × 10.44 Å × 33.56 Å) with a solution region of 20 Å. Edge surfaces perpendicular to [010], [0$\bar{1}$0], [110], and [$\bar{1}\bar{1}$0] crystallographic directions were modeled. The solution region contained 130 water molecules, approximately corresponding to the density of bulk water at ambient conditions (Figure S1). Ten water molecules were inserted into the interlayer to create a monolayer hydrate (Figure 2 as an example).

In the initial configuration, all surface O atoms were saturated with H atoms, and Al atoms were 6-fold coordinated (Figure 2). Structures without (No-sub) and with Mg^{2+} substitution (Mg-sub) were investigated. Due to the high computational cost, we only investigated the cases where Mg^{2+} substitution occurs in the *cis*-octahedron (Figure S2).

2.2. First Principles Molecular Dynamics. CP2K/Quickstep package based on mixed Gaussian plane wave scheme was used to carry out all simulations.[41] Perdew−Burke−Ernzerhof functional was applied for exchange correlation effects,[42] and Goedecker−Teter−Hutter pseudopotentials were used to represent the core electron state.[43] The dispersion correction was applied in all calculations with the Grimme-D3 method.[44,45] A double-ζ valence augmented with polarization basis set[46] was employed for H, O, Mg, Al, and Si, and the plane wave cutoff was set to be 400 Ry.

Born−Oppenheimer molecular dynamics simulations were carried out with a wave function optimization tolerance of 10^{-6}. Canonical ensemble (*NVT*) conditions were imposed using a Nóse−Hoover chain thermostat with a target temperature of 300 K.[47] The MD time step was set to be 0.5 fs. For each system, we conducted an initial equilibration simulation of 3.0 ps, followed by a production period of 5.0−10.0 ps.

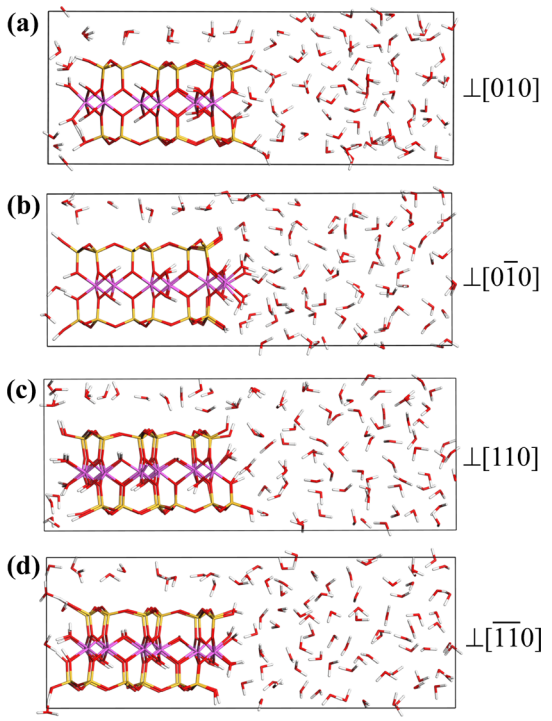

Figure 2. Edge surface model of non-substituted (No-sub) cis-vacant structure. (a) ⊥[010], (b) ⊥[0$\bar{1}$0], (c) ⊥[110], and (d) ⊥[$\bar{1}\bar{1}$0]. Color scheme: Si (yellow), Al (pink), O (red), H (white).

2.3. Acidity Constant Calculations. The pK_a values of the edge surface sites were computed using the half-reaction scheme of the FPMD-based vertical energy gap method.[48,49] In this method, the proton of an acid (denoted as AH) is gradually transformed into a ghost atom, and the free energy of the transformation is calculated according to the thermodynamic integration approach. Full details are given in the Supporting Information.

The investigated edge surface sites were ≡Al/Mg$(OH_2)_2$, ≡Al/Mg(OH_2)OH, ≡Si(OH), ≡Al(OH_2), ≡Si$(OH)_2$Al/Mg, ≡SiO(OH)Al/Mg, and ≡Al/Si/Mg(OH)Al for the surfaces perpendicular to [010], [0$\bar{1}$0], [110], and [$\bar{1}\bar{1}$0] (Figures 2 and S2). The slashes represent the different octahedral or tetrahedral connection sites. Dangling O atoms at the surface sites usually require two H atoms to saturate. Doubly protonated silanol sites ≡Si(OH_2) do not exist in the normal pH range and do not contribute to the acid−base chemistry, and thus were not considered.[23] For some sites, for example, ≡Si$(OH)_2$Al on the surface perpendicular to [010], one proton dissociated spontaneously within a few picoseconds in free simulations. Therefore, the O−H bonds were restrained in pK_a calculations of these sites (Tables S1 and S2). For some sites, for example, ≡Al/Mg(OH)Al and ≡Mg$(OH_2)_2$, the deprotonated forms would capture one proton from water molecule. For the calculations of these sites, all OH bonds of water molecules were restrained at 1.89 bohr to prevent this from happening in the simulation.

2.4. Surface Complexation Modeling. A modified version of PHREEQC that considers the spillover of electrostatic potential from basal surfaces was used to construct SCMs for clay layer edge surfaces.[5,21,50] A key feature is that the electrostatic potential of edge surfaces is negative when the edge surface charge is zero. PHREEQC scripts and database are available in the Supporting Information.

https://doi.org/10.1021/acs.est.2c07171
Environ. Sci. Technol. 2023, 57, 1342−1352

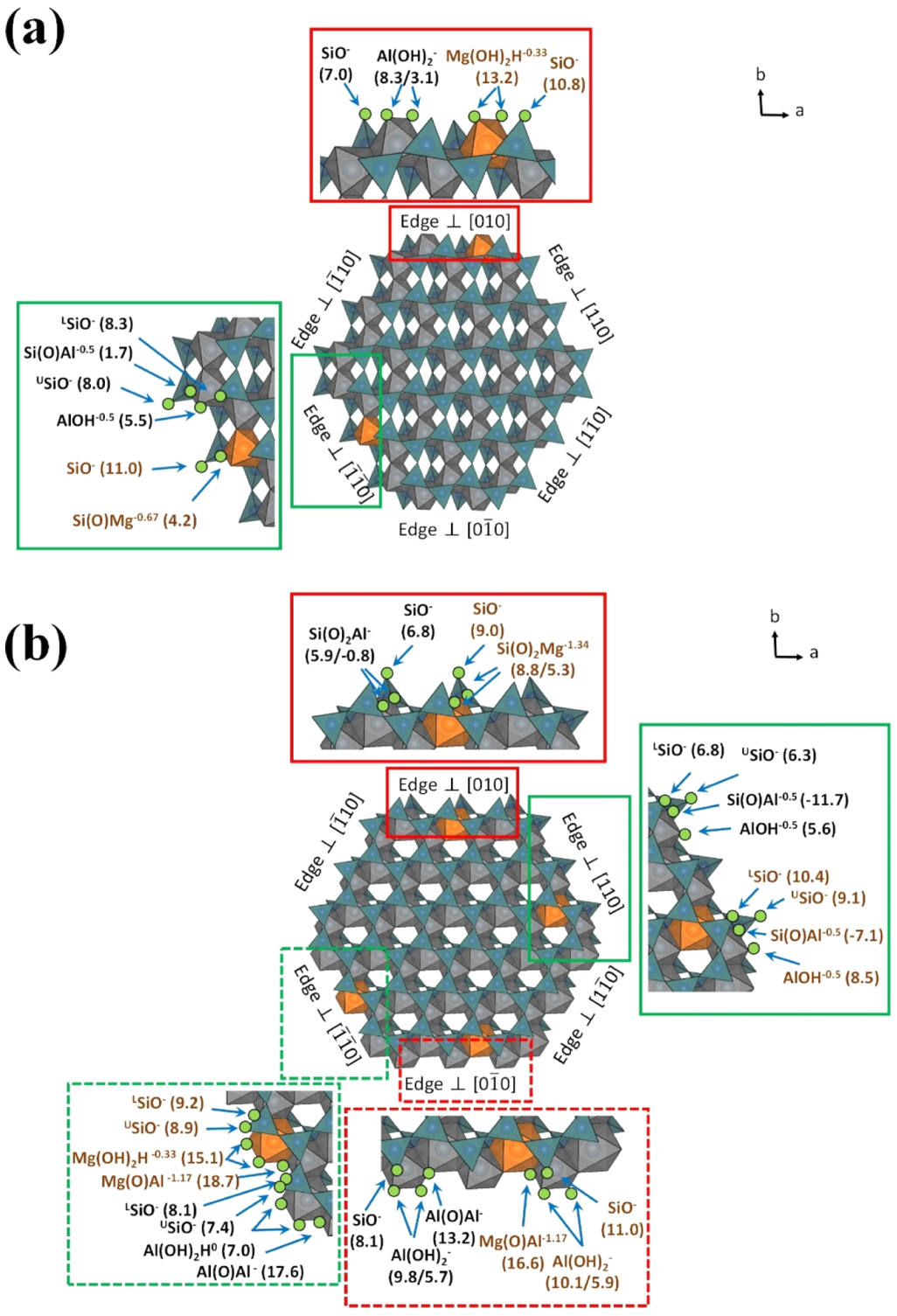

Figure 3. Edge surface sites and pK_a values of trans-(a) and cis-(b) vacant clay models. The pK_a values of trans-vacant clay model were taken from Liu et al.[23]

3. RESULTS AND DISCUSSION

3.1. FPMD Simulations. *3.1.1. Surface Structures of Cis-Vacant Model.* Compared with the trans-vacant model, the surface perpendicular to [010] of cis-vacant model has a special structure with symmetrical vacancy surrounded by ≡Si(OH)$_2$Al/Mg and ≡Si(OH) (Figure 2a). Vacancy usually serves as an adsorption site for heavy metals.[51−53] Similar to the trans-vacant edge perpendicular to [010] direction, the cis-vacant model also has ≡Al(OH$_2$)$_2$ and ≡Si(OH) sites on [0$\bar{1}$0] direction (Figure 2b). Both surfaces perpendicular to [110] and [$\bar{1}$10] on the cis-vacant model are inclined edges which are similar to the trans-vacant edge perpendicular to [110]. Such beveled surfaces have different silanol groups, that is, ≡Si(OH)^U (silanol on upper T-sheet) and ≡Si(OH)^L (silanol on lower T-sheet). For edge perpendicular to [$\bar{1}$10], there are ≡Al(OH$_2$)$_2$ and ≡Al(OH)Al sites (Figure 2c). In

https://doi.org/10.1021/acs.est.2c07171
Environ. Sci. Technol. 2023, 57, 1342−1352

Table 1. Summary of pK_a Values of Edge Sites on Individual Surfaces of Trans/Cis-Vacant Models (tv and cv, Respectively)[a]

	sites	tv ⊥ [010]	tv ⊥ [110]	cv ⊥ [010]	cv ⊥ [0$\bar{1}$0]	cv ⊥ [110]	cv ⊥ [$\bar{1}$10]
No-sub	≡Si(OH)	7.0	$8.0^{U}/8.3^{L}$	6.8	8.1	$6.3^{U}/6.8^{L}$	$7.4^{U}/8.1^{L}$
	≡Al$(OH_2)_2$	3.1			5.7		7.0
	≡Al(OH)(OH_2)	8.3			9.8		
	≡Al(OH_2)		5.5			5.6	
	≡Si(OH)Al		1.7			−11.7	
	≡Si$(OH)_2$Al			−0.8			
	≡Si(O)(OH)Al			5.9			
	≡Al(OH)Al				13.2		17.6
Mg-sub	≡Si(OH)	10.8	11.0	9.0	11.0	$9.1^{U}/10.4^{L}$	$8.9^{U}/9.2^{L}$
	≡Mg$(OH_2)_2$	13.2					15.1
	≡Si(OH)Mg		4.2				
	≡Al$(OH_2)_2$				5.9		
	≡Al(OH)(OH_2)				10.1		
	≡Al(OH_2)					8.5	
	≡Si(OH)Al					−7.1	
	≡Si$(OH)_2$Mg/≡Si(O)(OH)Mg			5.3/8.8			
	≡Mg(OH)Al				16.6		18.7

[a]The pK_a values of the trans-vacant model were taken from Liu et al.[23]

addition, the edge perpendicular to [110] has the same type of surface sites (i.e., ≡Al(OH_2) and ≡Si(OH)Al) (Figure 2d) as the trans-vacant edge perpendicular to [110]. In the case of Mg^{2+} substitution, ≡Si$(OH)_2$Mg and ≡Mg$(OH_2)_2$ appeared on surfaces perpendicular to [010] and [$\bar{1}$10], while the surface sites on surfaces perpendicular to [0$\bar{1}$0] and [110] are the same to the No-sub model because the cis-octahedron substituted by Mg^{2+} is inside the bulk phase (Figure S2).

3.1.2. Acidity Constant of Cis-Vacant Model. The pK_a values of all edge surface sites for the non-substituted (No-sub) and Mg-substituted (Mg-sub) models were computed with statistical uncertainties within 1.6 pK_a units (Tables S3 and S4). The uncertainties of the pK_a value were evaluated as the semi-difference between the value using the first half of the trajectory only and the second half of the trajectory only. Figure S3 shows the accumulating averages of vertical energy gaps of ≡Al$(OH_2)_2$ on the edge perpendicular to [$\bar{1}$10] and ≡Si(OH) on the edge perpendicular to [0$\bar{1}$0], which indicated that the results converged within the simulation period, and the effect of possible dipole was negligible.

On the surface perpendicular to [010], ≡Si$(OH)_2$Al site had the lowest pK_a (−0.8), indicating that the site is mostly deprotonated at a common pH value. Proton dissociation at ≡Si$(OH)_2$Al site increased the pK_a of ≡SiO(OH)Al to 5.9, suggesting that ≡SiO(OH)Al and ≡SiO(O)Al are dominant surface species under environmentally relevant conditions. The ≡Si(OH) site had a pK_a of 6.8, which was similar to the pK_a of 7.0 of the silanol on the trans-vacant model (Figure 3a).[23] Furthermore, the pK_a values of ≡Si(OH) site on the edge perpendicular to [0$\bar{1}$0] and the bound water at ≡Al$(OH_2)_2$/≡Al(OH)(OH_2) sites were 8.1 and 5.7/9.8, respectively. These results were also consistent with the similar sites (≡Si(OH), ≡Al$(OH_2)_2$ and ≡Al(OH)(OH_2)) on the trans-vacant edge perpendicular to [010] considering the model calculation error margin. The ≡Al(OH)Al site on the edge perpendicular to [0$\bar{1}$0] had a pK_a value of 13.2, indicating that it remained protonated even at high pH values.

On the surface perpendicular to [110], the pK_a values of ≡Si$(OH)^{U}$ and ≡Si$(OH)^{L}$ were 6.3 and 6.8, close to the values obtained for the silanols on the edge perpendicular to [$\bar{1}$10](i.e., 7.4 and 8.1, respectively) (Figure 3b). A similar result has been described for silanol sites on trans-vacant surface (i.e., 8.0 vs 8.3 for ≡Si$(OH)^{U}$ and ≡Si$(OH)^{L}$ sites).[23] Similar to the trans-vacant model, ≡Si(OH)Al on the edge perpendicular to [110] had a pK_a of −11.7, implying that it was unstable in the presence of water. ≡Al(OH_2) site on the edge perpendicular to [110] and ≡Al$(OH_2)_2$ on the edge perpendicular to [$\bar{1}$10] of cis-vacant model had pK_a values of 5.6 and 7.0, respectively, which were close to the ≡Al(OH_2) site on the trans-vacant edge perpendicular to [110] (i.e., pK_a of 5.5).[23] For ≡Al(OH)Al site on the edge perpendicular to [$\bar{1}$10] (i.e., the structural OH), the pK_a value was 17.6, indicating that it should not contribute to edge surface acid−base properties.

Previous studies show that the influence of isomorphic substitution on surface pK_a values is usually limited in one unit cell.[23,25] In our cis-vacant model, Mg^{2+} substitution took place in the first octahedral layer on the surface perpendicular to [010] (Figure S2a). The pK_a of the ≡Si(OH) site connected with Mg via bridging oxygen was 9.0, while the pK_a values of ≡Si$(OH)_2$Mg and ≡SiO(OH)Mg sites were 5.3 and 8.8, respectively (Figure 3b). Therefore, ≡Si$(OH)_2$Mg can contribute to the titration data, which is in contrast to the ≡Si$(OH)_2$Al site on the No-sub model described previously. All of the pK_a values were higher than their counterparts on the No-sub model, similar to the finding for trans-vacant surfaces. On the surface perpendicular to [0$\bar{1}$0], the edge surface sites have the same nomenclature as on No-sub surface except that they connect with Mg via bridge oxygen. The ≡Si(OH) site had a pK_a of 11.0, which was consistent with the Mg-sub trans-vacant edge perpendicular to [010] (10.8). However, the pK_a values of ≡Al$(OH_2)_2$ and ≡Al(OH_2)(OH) sites were 5.9 and 10.1, respectively, which were close to the values of their counterparts on the No-sub model (i.e., 5.7 and 9.8), suggesting that the effect of Mg^{2+} substitution on Al sites is weak. ≡Mg(OH)Al site had a very high pK_a of 16.6 and therefore should be protonated in water.

Similar effect of Mg-sub has been found for the other surfaces. ≡Si$(OH)^{U}$ and ≡Si$(OH)^{L}$ sites on the Mg-sub cis-vacant edge perpendicular to [110] had pK_a values of 9.1 and 10.4, respectively, which were higher than their counterparts on the No-sub model (Figure 3b). The ≡Al(OH_2) site was

https://doi.org/10.1021/acs.est.2c07171
Environ. Sci. Technol. 2023, 57, 1342−1352

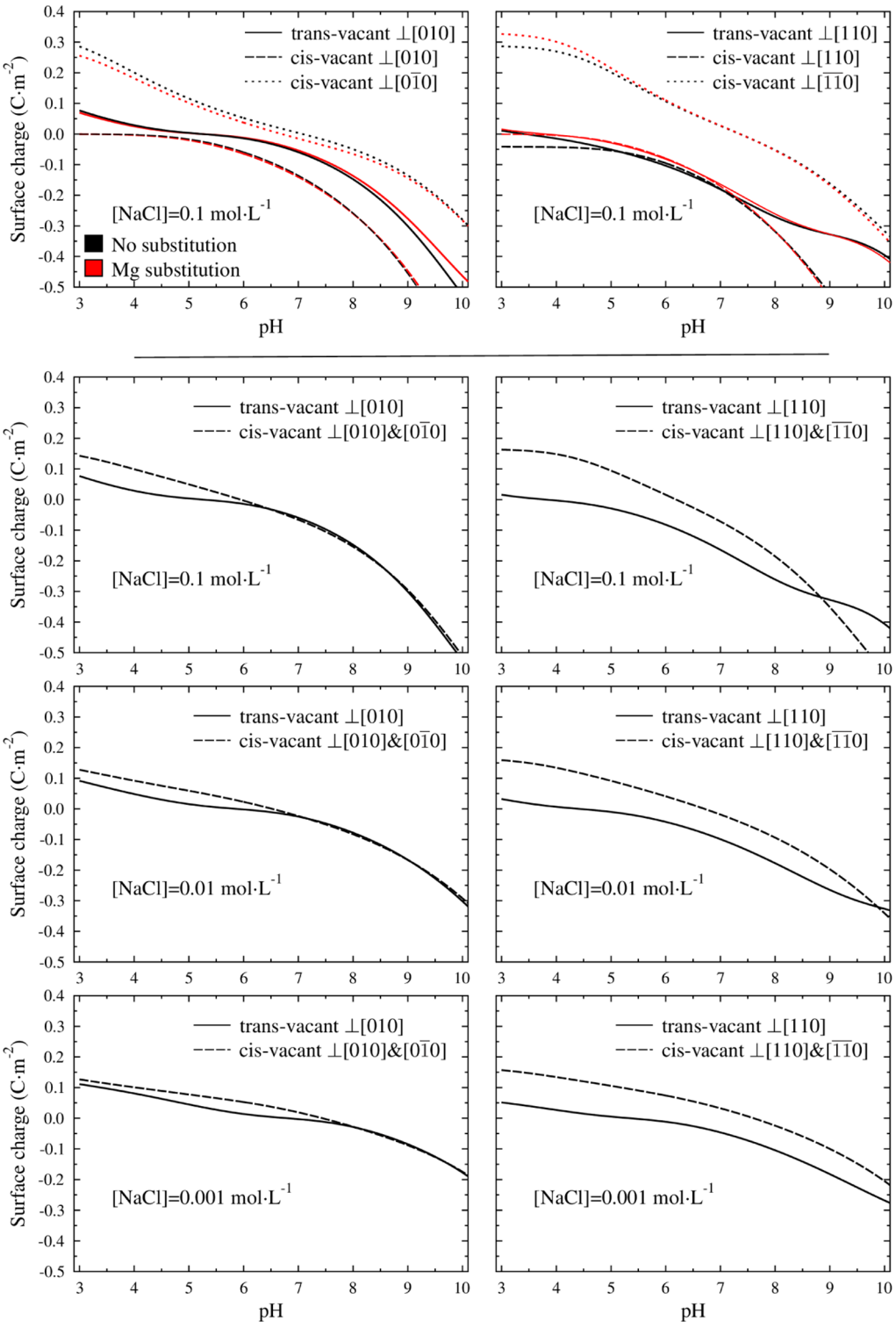

Figure 4. Comparison of the predicted titration model for No/Mg-sub cis- and trans-vacant structure on edges perpendicular to [010]/[0$\bar{1}$0] and [110]/[$\bar{1}$10]. The specific edge surface area was set to 14 $m^2 \cdot g^{-1}$ and both the relative abundance of edges perpendicular to [010], [0$\bar{1}$0], [110], and [$\bar{1}$10] were set to 1/1 respectively. The fractions of Mg substitution were set to 0.125.

mostly protonated under a neutral pH (pK_a of 8.5), while ≡Si(OH)Al site was deprotonated (pK_a of −7.1). On the surface perpendicular to [$\bar{1}$10] of the Mg-sub model, the pK_a values of ≡Si(OH)^U and ≡Si(OH)^L sites increased slightly to 8.9 and 9.2 compared to the No-sub model (i.e., 7.4 and 8.1, respectively). ≡Mg(OH$_2$)$_2$ and the structural OH site (i.e., ≡Mg(OH)Al) were inert because of their high pK_as (15.1 and 18.7, respectively).

The pK_a values in Table 1 form a complete set of acidity constants for Al−Mg montmorillonite edge surface sites. A cis-vacant model has more diverse sites than a trans-vacant model. For example, ≡Si(OH)$_2$Al was the unique site on edge surfaces on the cis-vacant model, and it was the major reactive

https://doi.org/10.1021/acs.est.2c07171
Environ. Sci. Technol. 2023, 57, 1342−1352

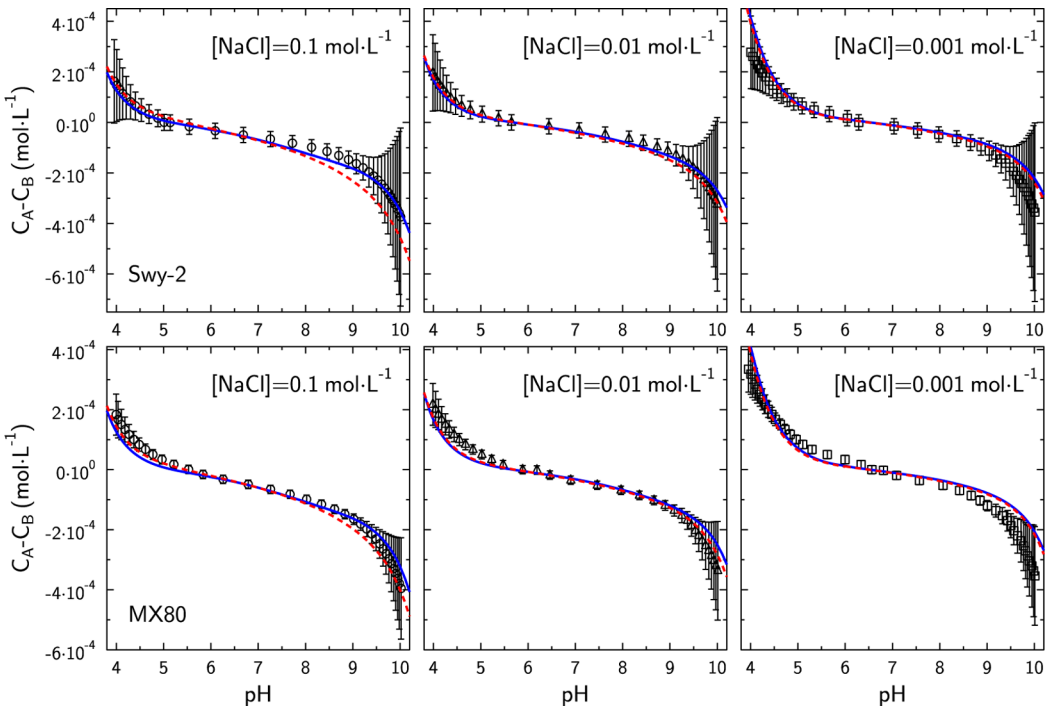

Figure 5. Comparison of model predictions (lines) and potentiometric titration data (symbols) for MX80 montmorillonite (bottom) and SWy-2 montmorillonite (top) as reported by Tournassat et al.[21] The specific edge surface area was set to 12 and 14 $m^2 \cdot g^{-1}$ for, respectively, MX80 and Swy-2 montmorillonite as by Tournassat et al.[21] The relative abundance of edges perpendicular to [010] and [110] was set at 0.3/0.7 for the trans-vacant model (plain blue lines) and that of edges perpendicular to [010], [0$\bar{1}$0], [110], and [$\bar{1}$10] was set at 0.15/0.15/0.35/0.35 for the cis-vacant model (dashed red lines) in agreement with AFM results.[54]

site under ambient pH. Moreover, the structural OH sites (≡Al(OH)Al) on surfaces perpendicular to [0$\bar{1}$0] and [$\bar{1}$10] had extremely high pK_a values, which did not show reactivity at a common pH. Overall, these acidity results imply that ≡Si(OH), ≡$Al(OH_2)_2$/≡Al(OH)(OH_2), ≡Si(O)(OH)Al, and ≡$Al(OH_2)$ sites on edge surfaces of non-substituted cis-vacant layer are the major reactive sites, whereas the reactivity of trans-vacant layers mainly depends on ≡Si(OH), ≡$Al(OH_2)_2$/≡Al(OH)(OH_2), and ≡$Al(OH_2)$ sites. The distributions of dominant surface sites on No-sub cis-vacant edge surfaces are shown in Figure S4. Mg^{2+} substitution increased the pK_a values of neighboring sites, which can alter the acid chemistry of some sites (e.g., ≡$Si(OH)_2$Mg and ≡$Mg(OH_2)_2$).

3.2. Predicted SCM for Cis-Vacant Clay Minerals. Previous studies have established prediction models of the acid−base titration data, in which the acidity constants were based on the trans-vacant model,[21] and the results indicated that the surfaces perpendicular to the different crystallographic directions have different surface charges. For comparison, we employed two sets of pK_a values from the trans- and cis-vacant models to construct the SCM on different edge surfaces.

On the common edge surfaces of trans- and cis-vacant models (i.e., surface perpendicular to [010], [0$\bar{1}$0], [110], and [$\bar{1}$10] crystallographic directions), the surface charge decreased with increasing pH to a similar extent for the two models (Figure 4 top). Moreover, edge surface charge of both trans- and cis-vacant models had little dependence on Mg^{2+} substitutions, but the dependence on the crystal plane orientation was strong.

The averaged charge of surfaces perpendicular to [010], [0$\bar{1}$0], [110], and [$\bar{1}$10] in the cis-vacant model was compared to the charge of surfaces perpendicular to [010] and [110] in the trans-vacant model (Figure 4 bottom), respectively. At 0.1 $mol \cdot L^{-1}$ NaCl, the averaged charge of surfaces perpendicular to [010] and [0$\bar{1}$0] in the cis-vacant model was slightly higher than that of the surface perpendicular to [010] in the trans-vacant model at pH < 6.0 and identical to each other at higher pH values. The surface charges on cis-vacant surfaces perpendicular to [110] and [$\bar{1}$10] were higher than that of the trans-vacant surface perpendicular to [110] at pH < 8.8, but the surface charge of cis-vacant surfaces decreased with a larger slope than that of trans-vacant surface, leading to a more negative surface at pH above 8.8. Changes in ionic strength were predicted to have a significant effect on surface charge. Both cis- and trans-vacant models showed that a decrease in ionic strength results primarily in a reduction of the surface charge variation amplitude and in a shift of the point of zero charge toward higher pH values. The overall charge on all edge surfaces for cis- and trans-vacant structures was also calculated (Figure S5). The difference in the overall charge between cis-vacant and trans-vacant structures was mainly controlled by the apparent discrepancy between the trans-vacant surface perpendicular to [110] and cis-vacant surfaces perpendicular to [110] and [$\bar{1}$10] (Figure 4), and thus, their profiles were similar to one another.

We tested our cis-vacant model by comparing its predictions with published potentiometric titration data (Figure 5).[21,55] Proportions of edge surface directions were set at 0.3/0.7 for surfaces perpendicular to [010] and [110] in the trans-vacant model and 0.15/0.15/0.35/0.35 for the surfaces perpendicular to [010], [0$\bar{1}$0], [110], and [$\bar{1}$10] in the cis-vacant model, in agreement with atomic force microscopy (AFM) results, showing a predominance of edge surfaces perpendicular to [110] and [$\bar{1}$10] compared to those perpendicular to [010].[54] In the cis-vacant model, only octahedral Mg^{2+}/Al^{3+} and Fe^{2+}/

https://doi.org/10.1021/acs.est.2c07171
Environ. Sci. Technol. 2023, 57, 1342−1352

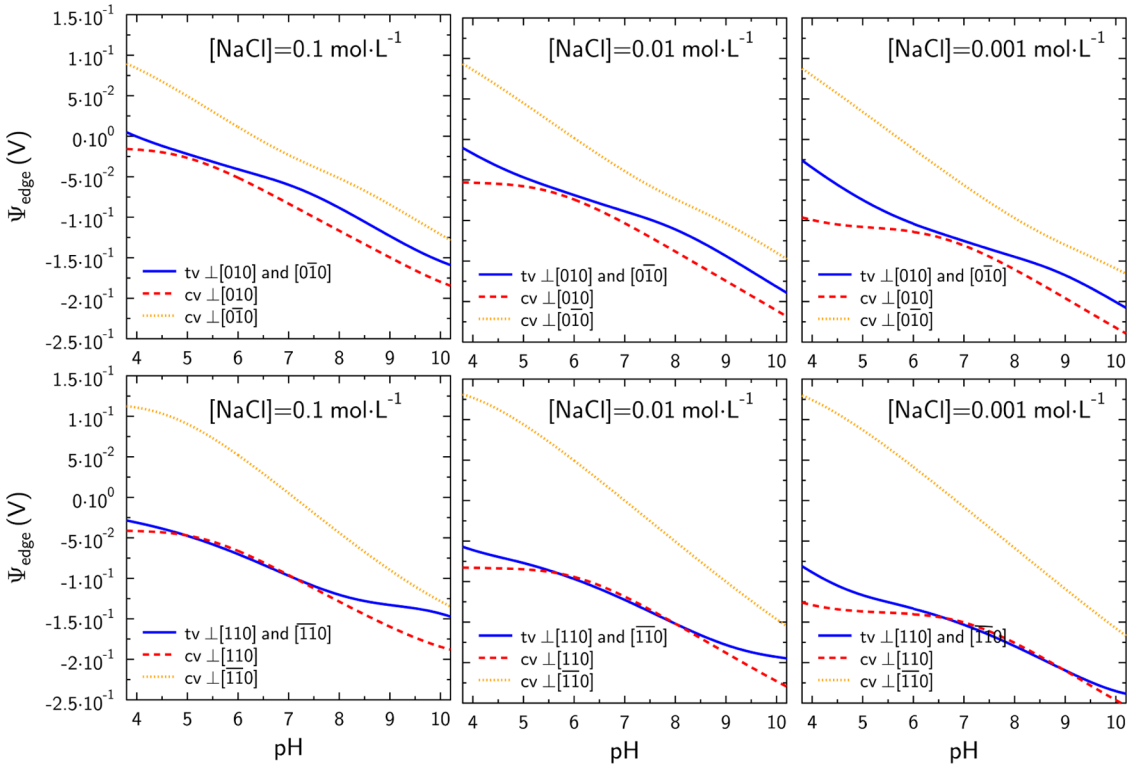

Figure 6. Swy-2 edge surface potentials as a function of surface directions, pH, and ionic strength. Comparison of our cis-vacant model and the trans-vacant model by Tournassat et al.[21]

Al^{3+} substitutions were taken into account. Sites with Fe^{2+}/Al^{3+} substitutions were considered to have the same pK_a parameters as the sites with Mg^{2+}/Al^{3+} substitutions, and Al^{3+}/Si^{4+} substitutions were not considered. All other model parameters and calculation procedures were identical to those used by Tournassat et al.[21] The consideration of a cis-vacant instead of a trans-vacant structure had a significant influence on the edge surface charge (Figure 4), but it had little effect on the prediction of potentiometric titration results (Figure 5). The agreement of the model with experimental data was not improved compared to the trans-vacant model. An almost perfect agreement with the experimental data can be achieved by adjusting the pK_a values of edge surface sites in the limit of the ±1.6pK_a unit uncertainty, but as already explained by Tournassat et al.,[21] such a refinement was not deemed justified in light of the uncertainties in the experimental data. This comparison highlights the lack of modeling constraint provided by potentiometric titration data. As already stated in the literature, contrary to oxi(hydr)oxides surfaces, potentiometric titration curves of montmorillonite measured as a function of ionic strength do not exhibit a crossover point,[12,55,56] because of the spillover effect of basal surface potential on edge surfaces. In addition, because of the predominance of the basal surfaces over the edge surfaces, electrophoretic measurements of Na-montmorillonite particles always result in negative ζ potential values.[57] Consequently, no point of zero charge of edge surfaces and iso-electric point can be determined accurately. At last, the smooth decrease of proton charge with pH does not allow the identification of individual pK_a values from the presence of inflexions in the titration curves. Nevertheless, we consider that our cis-vacant model is improved compared to the previously published trans-vacant model by Tournassat et al.,[21] because a good agreement between predicted and measured proton charge was found (Figure 5) and because our cis-vacant model takes into account the most recent insights on clay edge surface structure and reactivity. First, the cis-vacant structure at montmorillonite edges was confirmed with high resolution electron transmission microscopy measurements.[34] And second, relative proportions of edge surface directions were made available from AFM measurements.[54] Our cis-vacant model could be further improved with the addition of other types of substitutions, of which the pK_a values remain to be determined using FPMD calculations.

The trans-vacant model predicted a negative surface potential at pH above 4 for the two types of surfaces present in the model, that is, perpendicular to [010] and [110] (Figure 6). Contrastingly, the cis-vacant model predicted a negative surface potential at pH above 4 for surfaces perpendicular to [010] and [110] but a positive surface potential at pH below ∼6−7 for surfaces perpendicular to [0$\bar{1}$0] and [$\bar{1}$10]. Hence, for pH below 6−7, montmorillonite particles may exhibit edge surface with a positive surface potential on one side and a negative surface potential on the other side.

Some anions, including metalloids, sorb weakly but notably on montmorillonite surfaces. Arsenate—As(V)—adsorption is pH-dependent and exhibits a bell shape with an adsorption maximum at pH 6−7.[58,59] Our modeling findings makes it possible to give an explanation to this adsorption behavior. The maximum of adsorption corresponds to the presence of negatively charged aqueous $H_2AsO_4^-$ and $HAsO_4^{2-}$ species concomitantly with the presence of a positive surface potential on some of montmorillonite edge surfaces. At lower pH, As(V) species are dominated by the neutral species H_3AsO_4, which cannot interact electrostatically with the surface, while at higher pH, the electrostatic interaction between the negative

https://doi.org/10.1021/acs.est.2c07171
Environ. Sci. Technol. 2023, 57, 1342−1352

surface potential and the negatively charged As(V) aqueous species is unfavorable. Similar adsorption behavior may also be explained for other oxyanions such as aqueous As(III), Se(IV), and Mo(VI).[60]

The highly complex nature of clay mineral surface reactivity requires the application of multiple techniques to obtain insightful parameters for the building of predictive SCMs.[6] Because of the complexity of the structure and chemistry on edge surfaces of montmorillonite, pK_a values cannot be obtained unequivocally from the fitting of potentiometric titration experiments,[12,56] and information gained at atomistic scale is necessary to build a constrained SCM. A key finding in the present study is related to the necessity to consider contrasted electrostatic properties at montmorillonite edge surfaces with various crystallographic directions in a single particle which arise from the non-centrosymmetric nature of montmorillonite cis-vacant layer structure.

■ ASSOCIATED CONTENT

Supporting Information

The Supporting Information is available free of charge at https://pubs.acs.org/doi/10.1021/acs.est.2c07171.

30 pages, including 4 tables and 5 figures; details on the method to calculate acidity constants; PHREEQC input files for cis-vacant structure; PHREEQC input files for trans-vacant structure (PDF)

■ AUTHOR INFORMATION

Corresponding Authors

Xiandong Liu − *State Key Laboratory for Mineral Deposits Research, School of Earth Sciences and Engineering, Nanjing University, Nanjing 210093, China; Frontiers Science Center for Critical Earth Material Cycling, Nanjing University, Nanjing 210023, China;* orcid.org/0000-0003-3966-3998; Email: xiandongliu@nju.edu.cn

Christophe Tournassat − *Institut des Sciences de la Terre d'Orléans, Université d'Orléans-CNRS-BRGM, Orléans 45071, France; Earth and Environmental Sciences Area, Lawrence Berkeley National Laboratory, Berkeley, California 94720, United States;* orcid.org/0000-0003-2379-431X; Email: christophe.tournassat@univ-orleans.fr

Authors

Pengyuan Gao − *Radiochemistry Laboratory, School of Nuclear Science and Technology, Lanzhou University, Lanzhou 730000, China; Frontiers Science Center for Rare Isotopes, Lanzhou University, Lanzhou 730000, China; Institut des Sciences de la Terre d'Orléans, Université d'Orléans-CNRS-BRGM, Orléans 45071, France;* orcid.org/0000-0002-8499-9274

Zhijun Guo − *Radiochemistry Laboratory, School of Nuclear Science and Technology, Lanzhou University, Lanzhou 730000, China; Frontiers Science Center for Rare Isotopes, Lanzhou University, Lanzhou 730000, China*

Complete contact information is available at: https://pubs.acs.org/10.1021/acs.est.2c07171

Notes

The authors declare no competing financial interest.

■ ACKNOWLEDGMENTS

P.G. was supported by the China Scholarship Council (grant no. 202006180105). P.G. acknowledges the Supercomputing Center of Lanzhou University and the CaSciMoDoT − Leto Supercomputing facilities of Region Centre Val de Loire, France. P.G. and Z.G. acknowledge funding from the National Natural Science Foundation of China (grant no. 12175094). C.T. acknowledges funding from the EC Horizon 2020 project EURAD under grant agreement 847593 (WP FUTURE). C.T.'s research at LBNL was supported by the U.S. Department of Energy, Office of Science, Office of Basic Energy Sciences, Chemical Sciences, Geosciences, and Biosciences Division, through its Geoscience program at LBNL under Contract DE-AC02-05CH11231. C.T. acknowledges a grant overseen by the French National Research Agency (ANR) as part of the "Investissements d'Avenir" program, LabEx VOLTAIRE, 10-LABX-0100 at ISTO. X.L. was supported by the National Natural Science Foundation of China (nos. 42125202 and 41872041) and is grateful to the High Performance Computing Center (HPCC) of Nanjing University for doing the numerical calculations in this paper on its blade cluster system.

■ REFERENCES

(1) Kome, G. K.; Enang, R. K.; Tabi, F. O.; Yerima, B. P. K. Influence of Clay Minerals on Some Soil Fertility Attributes: A Review. *Open J. Soil Sci.* **2019**, *09*, 155−188.

(2) Bergaya, F.; Lagaly, G. Chapter 1 General Introduction: Clays, Clay Minerals, and Clay Science. In *Developments in Clay Science*; Bergaya, F., Theng, B. K. G., Lagaly, G., Eds.; Elsevier, 2006; Vol. *1*, pp 1−18.

(3) Sposito, G.; Skipper, N. T.; Sutton, R.; Park, S.; Soper, A. K.; Greathouse, J. A. Surface Geochemistry of the Clay Minerals. *Proc. Natl. Acad. Sci. U.S.A.* **1999**, *96*, 3358−3364.

(4) Tournassat, C.; Bourg, I. C.; Steefel, C. I.; Bergaya, F. Chapter 1—Surface Properties of Clay Minerals. In *Developments in Clay Science*; Tournassat, C., Steefel, C. I., Bourg, I. C., Bergaya, F., Eds.; Elsevier, 2015; Vol. *6*, pp 5−31.

(5) Tournassat, C.; Tinnacher, R. M.; Grangeon, S.; Davis, J. A. Modeling Uranium(VI) Adsorption onto Montmorillonite under Varying Carbonate Concentrations: A Surface Complexation Model Accounting for the Spillover Effect on Surface Potential. *Geochim. Cosmochim. Acta* **2018**, *220*, 291−308.

(6) Liu, X.; Tournassat, C.; Grangeon, S.; Kalinichev, A. G.; Takahashi, Y.; Marques Fernandes, M. Molecular-Level Understanding of Metal Ion Retention in Clay-Rich Materials. *Nat. Rev. Earth Environ.* **2022**, *3*, 461−476.

(7) Lagaly, G. Chapter 5 Colloid Clay Science. In *Developments in Clay Science*; Bergaya, F., Theng, B. K. G., Lagaly, G., Eds.; Elsevier, 2006; Vol. *1*, pp 141−245.

(8) Davis, J. A.; James, R. O.; Leckie, J. O. Surface Ionization and Complexation at the Oxide/Water Interface. *J. Colloid Interface Sci.* **1978**, *63*, 480−499.

(9) Mccabe, R. W.; Adams, J. M. Chapter 4.3 - Clay Minerals as Catalysts. In *Developments in Clay Science*; Bergaya, F., Lagaly, G., Eds.; Elsevier, 2013; Vol. *5*, pp 491−538.

(10) White, G. N. Analysis and Implications of the Edge Structure of Dioctahedral Phyllosilicates. *Clays Clay Miner.* **1988**, *36*, 141−146.

(11) Baeyens, B.; Bradbury, M. H. A Mechanistic Description of Ni and Zn Sorption on Na-Montmorillonite Part I: Titration and Sorption Measurements. *J. Contam. Hydrol.* **1997**, *27*, 199−222.

(12) Bourg, I. C.; Sposito, G.; Bourg, A. C. M. Modeling the Acid−Base Surface Chemistry of Montmorillonite. *J. Colloid Interface Sci.* **2007**, *312*, 297−310.

(13) Charlet, L.; Schindler, P. W.; Spadini, L.; Furrer, G.; Zysset, M. Cation Adsorption on Oxides and Clays: The Aluminum Case. *Aquat. Sci.* **1993**, *55*, 291−303.
(14) Duc, M.; Carteret, C.; Thomas, F.; Gaboriaud, F. Temperature Effect on the Acid−Base Behaviour of Na-Montmorillonite. *J. Colloid Interface Sci.* **2008**, *327*, 472−476.
(15) Duc, M.; Gaboriaud, F.; Thomas, F. Sensitivity of the Acid−Base Properties of Clays to the Methods of Preparation and Measurement. *J. Colloid Interface Sci.* **2005**, *289*, 139−147.
(16) Duc, M.; Thomas, F.; Gaboriaud, F. Coupled Chemical Processes at Clay/Electrolyte Interface: A Batch Titration Study of Na-Montmorillonites. *J. Colloid Interface Sci.* **2006**, *300*, 616−625.
(17) Tombácz, E.; Szekeres, M. Colloidal Behavior of Aqueous Montmorillonite Suspensions: The Specific Role of PH in the Presence of Indifferent Electrolytes. *Appl. Clay Sci.* **2004**, *27*, 75−94.
(18) Tombácz, E.; Szekeres, M. Surface Charge Heterogeneity of Kaolinite in Aqueous Suspension in Comparison with Montmorillonite. *Appl. Clay Sci.* **2006**, *34*, 105−124.
(19) Wanner, H.; Albinsson, Y.; Karnland, O.; Wieland, E.; Charlet, L.; Wersin, P. The Acid/Base Chemistry of Montmorillonite. *Radiochim. Acta* **1994**, *66*−*67*, 157−162.
(20) Zysset, M.; Schindler, P. W. The Proton Promoted Dissolution Kinetics of K-Montmorillonite. *Geochim. Cosmochim. Acta* **1996**, *60*, 921−931.
(21) Tournassat, C.; Davis, J. A.; Chiaberge, C.; Grangeon, S.; Bourg, I. C. Modeling the Acid−Base Properties of Montmorillonite Edge Surfaces. *Environ. Sci. Technol.* **2016**, *50*, 13436−13445.
(22) Liu, X.; Lu, X.; Cheng, J.; Sprik, M.; Wang, R. Temperature Dependence of Interfacial Structures and Acidity of Clay Edge Surfaces. *Geochim. Cosmochim. Acta* **2015**, *160*, 91−99.
(23) Liu, X.; Cheng, J.; Sprik, M.; Lu, X.; Wang, R. Surface Acidity of 2:1-Type Dioctahedral Clay Minerals from First Principles Molecular Dynamics Simulations. *Geochim. Cosmochim. Acta* **2014**, *140*, 410−417.
(24) Liu, X.; Cheng, J.; Sprik, M.; Lu, X.; Wang, R. Interfacial Structures and Acidity of Edge Surfaces of Ferruginous Smectites. *Geochim. Cosmochim. Acta* **2015**, *168*, 293−301.
(25) Liu, X.; Lu, X.; Sprik, M.; Cheng, J.; Meijer, E. J.; Wang, R. Acidity of Edge Surface Sites of Montmorillonite and Kaolinite. *Geochim. Cosmochim. Acta* **2013**, *117*, 180−190.
(26) Cheng, J.; Sprik, M. Acidity of the Aqueous Rutile TiO_2 (110) Surface from Density Functional Theory Based Molecular Dynamics. *J. Chem. Theory Comput.* **2010**, *6*, 880−889.
(27) Liu, X.; Cheng, J.; Lu, X.; Wang, R. Surface Acidity of Quartz: Understanding the Crystallographic Control. *Phys. Chem. Chem. Phys.* **2014**, *16*, 26909−26916.
(28) Liu, X.; Cheng, J.; Sprik, M.; Lu, X.; Wang, R. Understanding Surface Acidity of Gibbsite with First Principles Molecular Dynamics Simulations. *Geochim. Cosmochim. Acta* **2013**, *120*, 487−495.
(29) Sulpizi, M.; Gaigeot, M.-P.; Sprik, M. The Silica−Water Interface: How the Silanols Determine the Surface Acidity and Modulate the Water Properties. *J. Chem. Theory Comput.* **2012**, *8*, 1037−1047.
(30) Tazi, S.; Rotenberg, B.; Salanne, M.; Sprik, M.; Sulpizi, M. Absolute Acidity of Clay Edge Sites from Ab-Initio Simulations. *Geochim. Cosmochim. Acta* **2012**, *94*, 1−11.
(31) Tsipursky, S. I.; Drits, V. A. The Distribution of Octahedral Cations in the 2:1 Layers of Dioctahedral Smectites Studied by Oblique-Texture Electron Diffraction. *Clay Miner.* **1984**, *19*, 177−193.
(32) Brigatti, M. F.; Galan, E.; Theng, B. K. G. Chapter 2 Structures and Mineralogy of Clay Minerals. In *Developments in Clay Science*; Bergaya, F., Theng, B. K. G., Lagaly, G., Eds.; Elsevier, 2006; Vol. *1*, pp 19−86.
(33) Subramanian, N.; Whittaker, M. L.; Ophus, C.; Lammers, L. N. Structural Implications of Interfacial Hydrogen Bonding in Hydrated Wyoming-Montmorillonite Clay. *J. Phys. Chem. C* **2020**, *124*, 8697−8705.
(34) Orucoglu, E.; Grangeon, S.; Gloter, A.; Robinet, J.-C.; Madé, B.; Tournassat, C. Competitive Adsorption Processes at Clay Mineral Surfaces: A Coupled Experimental and Modeling Approach. *ACS Earth Space Chem.* **2022**, *6*, 144−159.
(35) Kéri, A.; Dähn, R.; Krack, M.; Churakov, S. V. Combined XAFS Spectroscopy and Ab Initio Study on the Characterization of Iron Incorporation by Montmorillonite. *Environ. Sci. Technol.* **2017**, *51*, 10585−10594.
(36) Tournassat, C.; Ferrage, E.; Poinsignon, C.; Charlet, L. The Titration of Clay Minerals: II. Structure-based Model and Implications for Clay Reactivity. *J. Colloid Interface Sci.* **2004**, *273*, 234−246.
(37) Bickmore, B. R.; Tadanier, C. J.; Rosso, K. M.; Monn, W. D.; Eggett, D. L. Bond-Valence Methods for PKa Prediction: Critical Reanalysis and a New Approach. *Geochim. Cosmochim. Acta* **2004**, *68*, 2025−2042.
(38) Bickmore, B. R.; Rosso, K. M.; Nagy, K. L.; Cygan, R. T.; Tadanier, C. J. Ab Initio Determination of Edge Surface Structures for Dioctahedral 2:1 Phyllosilicates: Implications for Acid−Base Reactivity. *Clays Clay Miner.* **2003**, *51*, 359.
(39) Leung, K.; Nielsen, I. M. B.; Criscenti, L. J. Elucidating the Bimodal Acid−Base Behavior of the Water−Silica Interface from First Principles. *J. Am. Chem. Soc.* **2009**, *131*, 18358−18365.
(40) Leung, K.; Criscenti, L. J. Predicting the Acidity Constant of a Goethite Hydroxyl Group from First Principles. *J. Phys.: Condens. Matter* **2012**, *24*, 124105.
(41) Lippert, G.; Hutter, J.; Parrinello, M. A Hybrid Gaussian and Plane Wave Density Functional Scheme. *Mol. Phys.* **1997**, *92*, 477−487.
(42) Perdew, J. P.; Burke, K.; Ernzerhof, M. Generalized Gradient Approximation Made Simple. *Phys. Rev. Lett.* **1997**, *78*, 1396.
(43) Goedecker, S.; Teter, M.; Hutter, J. Separable Dual-Space Gaussian Pseudopotentials. *Phys. Rev. B: Condens. Matter Mater. Phys.* **1996**, *54*, 1703−1710.
(44) Grimme, S.; Ehrlich, S.; Goerigk, L. Effect of the Damping Function in Dispersion Corrected Density Functional Theory. *J. Comput. Chem.* **2011**, *32*, 1456−1465.
(45) Grimme, S.; Antony, J.; Ehrlich, S.; Krieg, H. A Consistent and Accurate *Ab Initio* Parametrization of Density Functional Dispersion Correction (DFT-D) for the 94 Elements H-Pu. *J. Chem. Phys.* **2010**, *132*, 154104.
(46) VandeVondele, J.; Hutter, J. Gaussian Basis Sets for Accurate Calculations on Molecular Systems in Gas and Condensed Phases. *J. Chem. Phys.* **2007**, *127*, 114105.
(47) Martyna, G. J.; Klein, M. L.; Tuckerman, M. Nosé−Hoover Chains: The Canonical Ensemble via Continuous Dynamics. *J. Chem. Phys.* **1992**, *97*, 2635−2643.
(48) Costanzo, F.; Sulpizi, M.; Valle, R. G. D.; Sprik, M. The Oxidation of Tyrosine and Tryptophan Studied by a Molecular Dynamics Normal Hydrogen Electrode. *J. Chem. Phys.* **2011**, *134*, 244508.
(49) Cheng, J.; Liu, X.; VandeVondele, J.; Sulpizi, M.; Sprik, M. Redox Potentials and Acidity Constants from Density Functional Theory Based Molecular Dynamics. *Acc. Chem. Res.* **2014**, *47*, 3522−3529.
(50) Parkhurst, D. L.; Appelo, C. A. J. Description of input and examples for PHREEQC Version 3-A computer program for speciation, batch-reaction, one-dimensional transport, and inverse geochemical calculations. *U.S. Geological Survey Techniques and Methods*; U.S. Geological Survey: Denver, CO, 2013; chapter A43, p 497, Book 6 , (available only at http://pubs.usgs.gov/tm/06/a43/)
(51) Zhang, C.; Liu, X.; Lu, X.; He, M. Complexation of Heavy Metal Cations on Clay Edges at Elevated Temperatures. *Chem. Geol.* **2018**, *479*, 36−46.
(52) Zhang, C.; Liu, X.; Lu, X.; Meijer, E. J.; Wang, R. Understanding the Heterogeneous Nucleation of Heavy Metal Phyllosilicates on Clay Edges with First-Principles Molecular Dynamics. *Environ. Sci. Technol.* **2019**, *53*, 13704−13712.

https://doi.org/10.1021/acs.est.2c07171
Environ. Sci. Technol. 2023, 57, 1342−1352

(53) Zhang, C.; Liu, X.; Lu, X.; Meijer, E. J.; Wang, R. An Atomic-Scale Understanding of the Initial Stage of Nucleation of Heavy Metal Cations on Clay Edges. *Geochim. Cosmochim. Acta* **2019**, *248*, 161−171.
(54) Kraevsky, S. V.; Tournassat, C.; Vayer, M.; Warmont, F.; Grangeon, S.; Wakou, B. F. N.; Kalinichev, A. G. Identification of montmorillonite particle edge orientations by atomic-force microscopy. *Appl. Clay Sci.* **2020**, *186*, 105442.
(55) Duc, M.; Gaboriaud, F.; Thomas, F. Sensitivity of the acid-base properties of clays to the methods of preparation and measurement: 2. Evidence from continuous potentiometric titrations. *J. Colloid Interface Sci.* **2005**, *289*, 148−156.
(56) Tournassat, C.; Grangeon, S.; Leroy, P.; Giffaut, E. Modeling Specific pH Dependent Sorption of Divalent Metals on Montmorillonite Surfaces. A Review of Pitfalls, Recent Achievements and Current Challenges. *Am. J. Sci.* **2013**, *313*, 395−451.
(57) Leroy, P.; Tournassat, C.; Bernard, O.; Devau, N.; Azaroual, M. The electrophoretic mobility of montmorillonite. Zeta potential and surface conductivity effects. *J. Colloid Interface Sci.* **2015**, *451*, 21−39.
(58) Manning, B. A.; Goldberg, S. Modeling Arsenate Competitive Adsorption on Kaolinite, Montmorillonite and Illite. *Clays Clay Miner.* **1996**, *44*, 609−623.
(59) Manning, B. A.; Goldberg, S. Adsorption and Stability of Arsenic(III) at the Clay Mineral−Water Interface. *Environ. Sci. Technol.* **1997**, *31*, 2005−2011.
(60) Goldberg, S.; Forster, H.; Godfrey, C. Molybdenum Adsorption on Oxides, Clay Minerals, and Soils. *Soil Sci. Soc. Am. J.* **1996**, *60*, 425−432.

https://doi.org/10.1021/acs.est.2c07171
Environ. Sci. Technol. 2023, 57, 1342−1352